Journal of Cleaner Production 234 (2019) 157–170

Contents lists available at ScienceDirect

Journal of Cleaner Production

journal homepage: www.elsevier.com/locate/jclepro

Co-utilization of converter sludge-containing dedust wastewater in iron ore sintering to save fresh water, enhance quality and reduce pollution

Yaozu Wang [a, c], Jianliang Zhang [a, b], Zhengjian Liu [a, *], Chengbo Du [a], Johannes Schenk [c], Jiugang Shao [d], Yapeng Zhang [e]

[a] School of Metallurgical and Ecological Engineering, University of Science and Technology Beijing, 30th Xueyuan Road, Haidian District, Beijing, 100083, PR China
[b] School of Chemical Engineering, The University of Queensland, St Lucia, QLD, 4072, Australia
[c] Ferrous Metallurgy, Montanuniversitaet Leoben, Franz-Josef-Straße 18, Leoben, A-8700, Austria
[d] Han Steel Company of HBIS Group, Fuxing Road 232, Handan, 056016, Hebei province, PR China
[e] LTD Research Institute of Technology, Shougang Group CO., 69th Yangzhuang Street, Shijingshan District, Beijing, 100041, PR China

ARTICLE INFO

Article history:
Received 27 March 2019
Received in revised form
14 May 2019
Accepted 17 June 2019
Available online 21 June 2019

Handling Editor: Vladimir Strezov

Keywords:
Dedust wastewater
Converter sludge
Iron ore sintering
Harmful elements

ABSTRACT

Due to the high proportion of the steel output produced by oxygen converter, significant quantities of converter sludge (CS) and dedust wastewater (DW) are generated annually as waste materials. This study tries to achieve the co-utilization of converter sludge-containing dedust wastewater (CSDW) in iron ore sintering to save fresh water and emission reduction. Firstly, this study quantitatively characterized the mineralogical characteristics of the CS through X-ray diffraction (XRD-Rietveld) and scanning electron microscope (SEM-EDS). The results indicated that the iron oxides wrapped the metallic Fe, and other impurities such as CaO, MgO and $ZnFe_2O_4$ mixed in the way of physical accumulation. The mineral composition of CS was metallic iron (9.2%), wustite (47.5%), calcium carbonate (31.7%), magnesium ferrite (4.8%), and zinc ferrite (6.7%). Influence of CSDW concentration on the granulation performance and sintering indexes was systematically studied through a series of experiments. Research findings showed that the permeability firstly raised from 9.66 to 12.88 JPU and then reduced to 11.94 JPU, and reached the maximum when the CSDW concentration was 40%. Migration behaviors of harmful elements Zn, K, Na, and Cl have been studied based on experiments and thermodynamic calculations. Cl in DW plays an important role in promoting the removal of alkali metals. The catalytic mechanism can be summarized as the reaction of HCl, Cl_2 and alkali metal oxides (Na_2CO_3, K_2CO_2, $NaAlSi_2O_2$, and $KAlSi_2O_2$) to form NaCl and KCl. With this technology, the removal rate of ZnO, K_2O, and Na_2O increased from 23% to 74%, 13%–42%, 1%–34%, respectively. This study aims to propose a new method for the co-utilization of CSDW in iron ore sintering, which would be helpful to save fresh water and reducing emissions in the iron and steel industry.

© 2019 Elsevier Ltd. All rights reserved.

1. Introduction

Steel stands as one of the most widely used materials in the world across industries from construction to blacksmithing to sewing. As one of the essential industry, the iron and steel industry is the impact of China's national economic development (da Silva et al., 2018; Peng et al., 2018; Wang et al., 2017). World steel output reached 1808 million tons in 2018, up 112.7% from 2000, with growth in China contributes most of the rise as its total output share rose to 51.32% from 15.1%. Generally, technologies of steelmaking can be divided into basic oxygen furnace (converter), open-hearth steelmaking and electric steelmaking. Fig. 1 gives the proportion of the steel output produced by converter to the total output in some countries in 2017. The statistical results indicate that converter is the most important method to produce steel in the world, especially in China. During the operation of a converter, the high-pressure oxygen blown by lance plays an essential role in controlling the carbon content of the molten steel. Accordingly, a

* Corresponding author.
E-mail address: liuzhengjian@ustb.edu.cn (Z. Liu).

https://doi.org/10.1016/j.jclepro.2019.06.186
0959-6526/© 2019 Elsevier Ltd. All rights reserved.

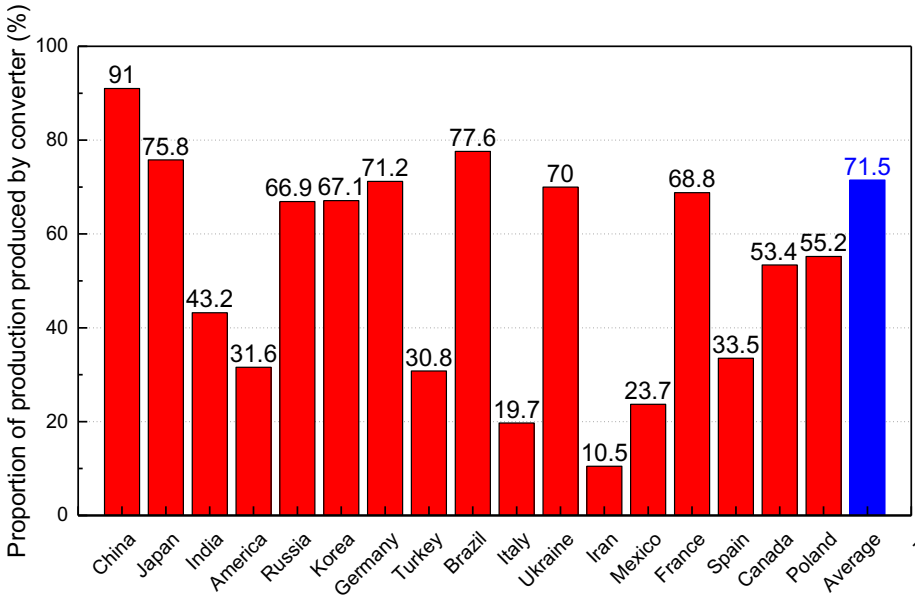

Fig. 1. The proportion of the steel output produced by converter to the total output in some countries in 2017 (World steel association, 2018).

large amount of CO, iron and other semi-metallic elements are generated and enter the wet dust removal system in form of flue gas. Under the treatment of the wet cleaning system, these dust are dispersed in the water to form the suspension liquid. After solid-liquid separation, the suspension liquid becomes the converter sludge (CS) with the water content of 30%~40%. It has been reported (Su et al., 2004a; Wu et al., 2012) that as many as 2–3 m^3 steel-making dedust wastewater (DW) and 15–20 kg CS can be obtained for every ton of steel produced.

Due to the high content of Ca^{2+}, DW is alkaline. At the same time, there is a large amount of water-soluble CO_2 (about 18%–30%) in the flue gas. CO_2 in flue gas could partially dissolve in water and form $CaCO_3$ precipitation, which indicates the high scaling possibility of the DW. Generally, DW in iron and steel enterprise is closed cycle for steelmaking, its complex treatment process greatly increases the cost of production. Previous studies also inferred that CS contained multiple metal oxides such as Fe_xO, Fe_3O_4, MgO, Al_2O_3, and MnO, which could be a potential secondary resource in preparing iron ore sintering (Agrawal and Pandey, 2005; Das et al., 2007; Denk et al., 2015; Nolasco-Sobrinho et al., 2003), combined flux (Lei and Li, 2015), iron powder (Aihua et al., n.d.), zinc oxide powder (Cantarino et al., 2012), Li(Fe, M)PO_4/C (Zhang et al., 2013), soil remediation agent (Melali and Shariatmadari, 2008) and water adsorbent (Leiviskä et al., 2017), as shown in Fig. 2. However, CS also has a high content of hazardous substances, such as ZnO, PbO, K_2O, and Na_2O. Due to the low volatility temperatures of Zn, Pb, K, and Na, these metals are easy to form dust and destroy the ecological environment. Among all the technologies, the utilization of CS in iron ore sintering is the most common and efficient way. Take China: the output of sinter in 2017 was 1142 million tons. At least 11 million tons of CS can be reused annually if 1% of CS is utilized per ton of sinter. It has been reported that the utilization of CS in iron ore sintering can replace parts of the iron ore and the flux, which is conducive to energy saving and consumption reduction (Agrawal and Pandey, 2005; Das et al., 2007; Denk et al., 2015; Nolasco-Sobrinho et al., 2003).

As summarized in Fig. 3, CS utilization for iron ore sintering can be divided into three forms according to different addition methods: (a) directly use as the raw material; (b) mini-pelletized sintering; (c) technology of hydraulic fill pipeline. As shown in Fig. 3 (a), Ren et al. (Ren et al., 1998; Y. Su et al., 2004b; Zhao and Zhu, 2004) mixed lime and CS together to absorb the water in CS and generate calcium hydroxide. Their studies indicated that by adding 4% of CS in the mixture could reduce the coke consumption

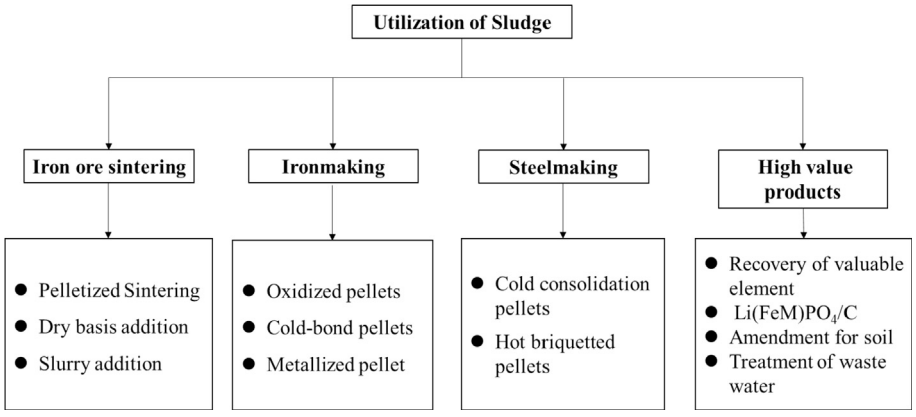

Fig. 2. Outline of CS treatment technologies.

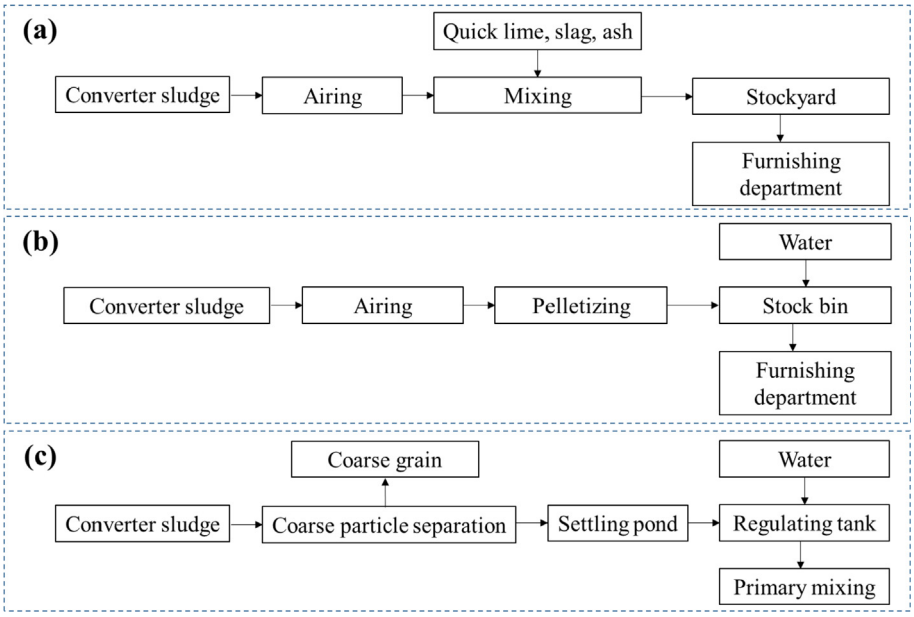

Fig. 3. Treatment schemes of CS in iron ore sintering.

by 1 kg/t and increase iron content, while the drum strength basically remained unchanged. However, the fluctuation of CaO and water brought difficulties to sintering production and made the composition of sinter fluctuate greatly. Wang et al. (2015) recycled CS by mini-pelletized sintering method. They made CS into pellets with the sizes of 3–10 mm first, and then spread the pellets into the mixture uniformly. Jin et al. (Hao, 2005; Jin and Liu, 2006) diluted CS with water into slurry with a concentration of 35–55%, as shown in Fig. 3 (b). After being pressurized by the pump, the slurry was transported to the sintering mixture to provide the required moisture. The vertical sintering speed increased from 16.25 mm/min to 16.79 mm/min, and the output increased by 5%. Moreover, the tumbler strength increased from 78.12% to 79.38%, which indicated an improvement in sinter performance. CS utilization through iron ore sintering could improve sinter quality and reduce energy consumption by technology of hydraulic fill pipeline and mini-pelletized sintering. However, iron ore sintering has a low removal rate of harmful elements. Lanzerstorfer (Lanzerstorfer et al., 2015) indicated that Zn contained in the iron ore was hardly reduced through sintering, and the zinc in the dust was discharged with the off-gas to an extent of about 25% pot test. Theoretical analysis and experiments showed that all the technologies could effectively recycle CS. However, the fluctuation of CaO and H_2O in CS brought difficulties to the sintering production and made the sinter composition fluctuate greatly. Moreover, CS and DW contains various harmful elements, which will be circulated and accumulated in the blast furnace if it is directly recycled to the sintering and served as raw material for the ironmaking. Therefore, it is urgent to develop a new technology to reduce the composition fluctuation and restrict the harmful elements in sinter.

This paper aims to provide a new method for the co-utilization of converter sludge-containing dedust wastewater (CSDW) in iron ore sintering to save fresh water and overcome the problems of high composition fluctuate and high harmful elements in sinter. Firstly, this study provides results of the chemical composition, size distribution, and mineralogical characteristics of CS. The mineral composition of the CS was identified through quantitative characterization by X-ray diffraction (XRD-Rietveld). Then, the effect of CSDW concentration on moisture capacity and granulation performance was studied through a series of experiments. In addition, this paper discussed the influence of CSDW concentration on sinter mineral evolution and sinter indexes. The mineralogical constitution of the sinter was characterized through a scanning electron microscope (SEM) coupled to an energy dispersive X-Ray spectrometer (EDS). Finally, the migration behaviors of harmful elements Zn, K, Na, and Cl have been studied through experiments. The removal mechanisms of Zn, K, Na, and Cl were investigated based on the thermodynamic calculation. Furthermore, the catalysis mechanisms of Cl in the removal of K and Na was proposed and analyzed.

2. Materials and methods

2.1. Materials

All the raw material used in this study came from a sintering plant in China. Table 1 gives the chemical composition of the ore and the fluxes (quick-lime and limestone) determined by chemical analysis and fluorescence analysis (XRF-1800, Shimadzu, Kyoto, Japan). Table 2 and Table 3 illustrates the ash composition and industrial analysis of coke. The CS and DW were derived from a steelmaking plant in China. Different concentrations (0%, 7%, 15%, 20%, 25%, 30%, 40%, and 50%) of CSDW were prepared by mixing the CS and the DW together to replace the fresh water used in iron ore sintering.

2.2. Moisture capacity experiments

During the granulating process, proper moisture is required to generate capillary forces between particles. Water plays an essential role in promoting the mixture into a ball. Moisture capacity is usually used to evaluate the binding ability between the iron ore and water, as expressed in equation-1. γ_g indicates the moisture capacity of the ore, M_S (g) is the weight after absorption, and M is the dry basis weight (g). Fig. 4 gives the schematic diagram of the moisture capacity experimental facilities. In a typical experiment, iron ore was dried in an oven at the temperature of 105 °C for 5 h to remove the water. 30 g dried ore was introduced in the circular

Table 1
Raw material chemical analysis (mass, %).

Material	TFe	FeO	CaO	MgO	Al_2O_3	SiO_2	MnO	S	P	K_2O	Na_2O	Zn
Ore 1	61.7	0.28	0.11	0.12	2.94	2.33	0.33	0.04	0.35	0.04	0.04	0.002
Ore 2	58.4	0.42	0.10	0.19	4.31	2.87	0.21	0.04	0.34	0.03	0.03	0.002
Ore 3	57.1	0.38	0.26	0.16	1.69	2.94	0.06	0.02	0.13	0.03	0.03	0.003
Ore 4	61.4	0.56	0.12	0.10	1.41	2.22	0.07	0.01	0.15	0.04	0.04	0.003
Ore 5	65.4	0.70	0.13	0.09	2.76	0.99	0.29	0.03	0.27	0.04	0.03	0.003
Ore 6	63.0	0.56	0.18	0.27	3.41	2.89	0.43	0.06	0.26	0.02	0.01	0.003
Ore 7	66.0	26.9	0.31	0.96	0.44	4.05	0.04	0.09	0.03	0.12	0.04	0.001
Ore 8	67.4	27.1	1.51	4.26	0.48	2.09	0.06	0.35	0.03	0.01	0.02	0.005
Sinter return fines	57.9	5.91	7.06	1.15	2.51	3.14	0.35	0.19	0.26	0.12	0.11	0.050
Steelmaking slag	45.5	32.7	29.83	5.28	3.36	11.41	2.09	0.27	1.42	0.07	0.35	0.007
Quick-lime	–	–	71.00	2.20	1.40	3.01	–	–	–	0.23	0.13	0.01
Dolomite	–	–	43.50	22.00	1.10	3.43	–	–	–	0.21	0.11	0.01

Table 2
Ash composition and proportion of coke breeze (mass, %).

Ash composition							Proportion
SiO_2	Al_2O_3	CaO	MgO	Fe_2O_3	SO_2	P	
45.00	30.00	4.00	0.60	15.4	4.49	0.51	4.00

Table 3
Industrial analysis of coke breeze (wt%) and the constant-volume low calorific value.

Ad	Vd	FCd	Mad	$Q_{net,\ v,\ ad}/(kJ\cdot kg^{1})$
10.19	9.88	79.29	0.64	26189.68

$$\gamma_g = \frac{M_S - M}{M} \times 100\% \quad (1)$$

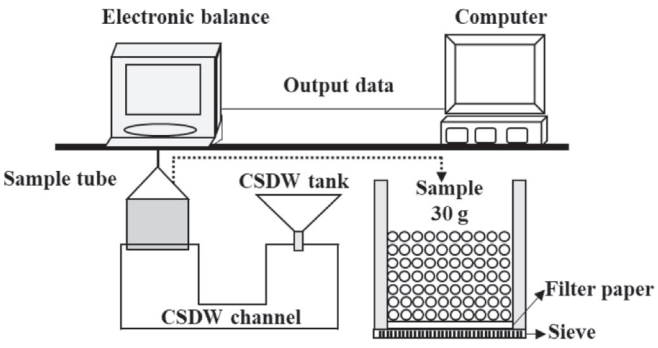

Fig. 4. Schematic diagram of the moisture capacity experimental facilities.

sample holder with a completely soaked filter paper at the bottom of the tube. Notably, the bottom of the tube was a sieve with 200 mesh. The imbibition tests were conducted by suspending the tube from an electronic balance and immersing it in CSDW. CSDW tank was used to maintain the liquid level. The computer recorded the mass data from the electronic balance. The experiment will come to an end until the mass keeps unchanged, which indicates that the water absorption of the ore reaches saturation. Take the average of the three experimental data as the final results.

$$\gamma_g = \frac{M_S - M}{M} \times 100\% \quad (1)$$

2.3. Granulating experiments

Series of experiments were conducted to understand the influence of CSDW on the granulating effect of the mixture. The schematic diagram of the granulating experiments was shown in Fig. 5. According to the experimental scheme (Table 4), the raw materials such as iron ore, flux, coke, and sinter return fines were mixed manually until well blended. Then the mixture was introduced to the drum granulator with a diameter of 257 mm, and a length of 585 mm. There are four feeding plates in the granulator, the section of which is trapezoid with a chamfering angle. The rotate speed of the granulator is 25r/min with the granulating time of 3 min. After the first granulation, a 3 min standing is necessary to ensure the full digestion of quicklime. Notably, the second granulation time was 5 min and the required water was the DW without CS. After the experiment, 1 kg of the mixture was used to measure the moisture content, another 1 kg mixture was used for the gas permeability experiments, and the rest of the mixture was used to measure the particle size composition. The mixture size group includes 7 grades (−0.25 mm, 0.25–1 mm, 1–2 mm, 2–3 mm, 3–6.13 mm, 6.13–8 mm, +8 mm). Carry out each test three times and take the mean to eradicate any discrepancies.

2.4. Description of sintering trials

As shown in Fig. 6, sintering trials were conducted in a sinter pot with a height of 800 mm and a diameter of 200 mm. A gas analyzer (MGA5) were placed in the bellows to measure the temperature, wind speed and chemical composition of sintering waste gas. 2 kg sinter with the size range between 10 mm and 12.5 mm was used as the bedding material. After granulation, the mixture was charged and then ignited at a temperature of 1050 ± 50 °C for 1.5 min with a suction pressure of 6 kPa. A suction pressure of 10 kPa was maintained during the sintering process. The schematic diagram of the sinter pot texts was listed in Fig. 6. In this research, the height of the material bed is 800 mm. The average of the three experimental data was taken as the final result.

2.5. Characterization

The chemical composition of CS and DW was determined by X-ray fluorescence (XRF), chemical analysis and inductively coupled plasma (ICP). The typical size distribution of the CS was determined by a laser particle size analysis (LMS-30) with a wavelength of

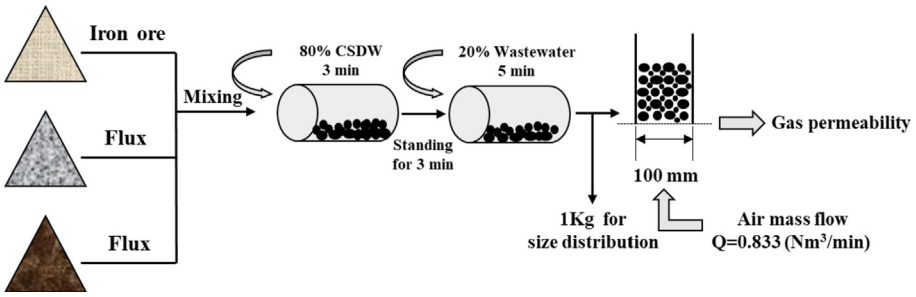

Fig. 5. Schematic diagram of the granulating experiments.

Table 4
Ore blend ratios of the sinter pot test (mass, %).

NO.	CSDW Concentration, %	CS	DW	Ore 1	Ore 2	Ore 3	Ore 4	Ore 5	Ore 6	Ore 7	Sinter return fines	Steelmaking slag	Quick-lime	Dolomite	Coke
1#	–	–	6.86	16.96	20.87	16.95	10.19	1.96	1.84	2.61	11.39	2.63	4.15	5.83	4.6
2#	7	0.52	6.61	16.96	20.77	16.85	10.09	1.96	1.74	2.51	11.39	2.63	4.15	5.84	4.6
3#	15	1.23	7.04	16.87	20.66	16.76	10.03	1.95	1.73	2.49	11.33	2.62	4.06	5.68	4.6
4#	20	1.74	6.97	16.80	20.58	16.69	9.99	1.94	1.72	2.48	11.29	2.61	4.00	5.56	4.6
5#	25	2.33	7.28	16.73	20.49	16.62	9.95	1.93	1.71	2.47	11.24	2.6	3.90	5.44	4.6
6#	30	2.98	7.13	16.64	20.39	16.54	9.90	1.92	1.7	2.46	11.18	2.59	3.82	5.28	4.6
7#	40	4.67	7.08	16.43	20.12	16.32	9.77	1.90	1.68	2.43	11.03	2.55	3.60	4.90	4.6
8#	50	6.97	7.13	16.13	19.77	16.03	9.60	1.86	1.65	2.38	10.84	2.51	3.28	4.38	4.6

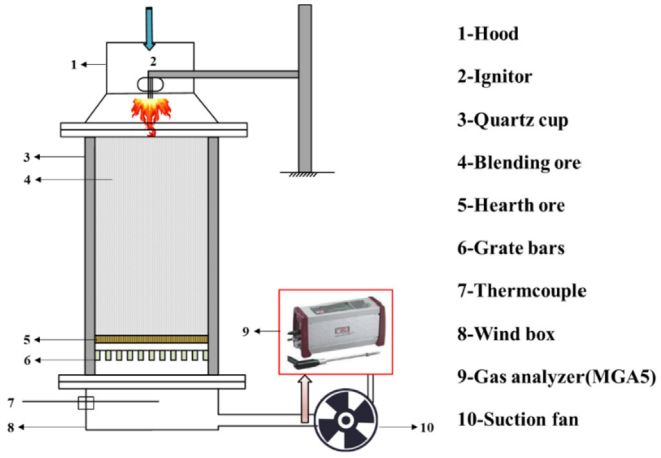

Fig. 6. Schematic diagram of the sinter pot test.

670 nm and a determination range 0.1–1000 μm. An ultrasonic water bath comprises the wet dispersion unit was used during the measurement. This study characterized the mineralogical characteristics of the ores and CS through X-ray diffraction (XRD-Rietveld) with Cu Kα radiation (M21XVHF22, MAC Science Co., Ltd., Japan) at a scanning speed of 4°/min and a step size of 0.01° over a range of 10–90°. In the process of multiphase refinement, the Chebyshev polynomial was used to fit the background. A scanning electron microscope (SEM, JSM-6701F) assisted with an energy dispersive X-Ray spectrometer (ESD) were used to observe the mineral characteristics and the microstructures of the sludge. The surface tension of CSDW with different concentrations was measured by Automatic surface tension tester (K100, KRUSS, Germany). The thermodynamic calculations are calculated by Factsage 7.2 with modules of Reaction.

3. Results and discussion

3.1. Characterization of CS and DW

3.1.1. Chemical composition

As summarized in Table 5, DW has a high content of Cl (909.1 mg/L) and Ca (43.76 mg/L). The hardness of the DW is relatively high, reaching 380 mg/L with a PH of 11.8. The chemical composition of CS is illustrated in Table 6. The results indicated that the main components are FeO, CaO, SiO_2, MgO, ZnO, Al_2O_3 and MnO. Due to the high level of Fe (49.67%) and CaO (25.45%) content, CS could be an excellent raw material in the iron and steel industries. It can be concluded that the content of Al_2O_3 and TiO_2 is much lower in CS than in iron ore, which makes it an excellent raw material for ironmaking and steelmaking. However, CS contains high levels of hazardous substances, such as ZnO (2.81%), K_2O (0.19%), and Na_2O (0.18%).

3.2. Size distribution

Fig. 7 gives the size distribution of CS. The results indicated that the grain size of the CS was very fine, and the proportion of the particles (<74 μm) accounted for more than 80%.

3.3. Quantitative analysis of mineral phases in CS

Fig. 8 illustrated the XRD-Rietveld analysis of the CS. The refinement significantly reduced the difference between the calculated pattern and the experimental pattern. There was no residual diffraction peak, which indicated that the crystal structure model was reasonable (Bartels et al., 1986). The R_{wp} of the refinement reached 6.25% with an accuracy of 1%, which indicated that

Table 5
Chemical composition and quality parameters of DW (mg/L).

Ca	Mg	Al	Hg	As	Cl	Hardness	Basicity	Total Fe	PH
43.76	0.65	0.56	0.11	0.06	909.10	380.00	112.00	0.84	11.80

Table 6
Chemical composition of CS (mass, %).

TFe	FeO	CaO	MgO	SiO_2	ZnO	MnO	Al_2O_3	TiO_2	K_2O	Na_2O	Cl
49.67	47.50	25.45	3.14	1.80	2.81	0.65	0.41	0.02	0.19	0.18	0.13

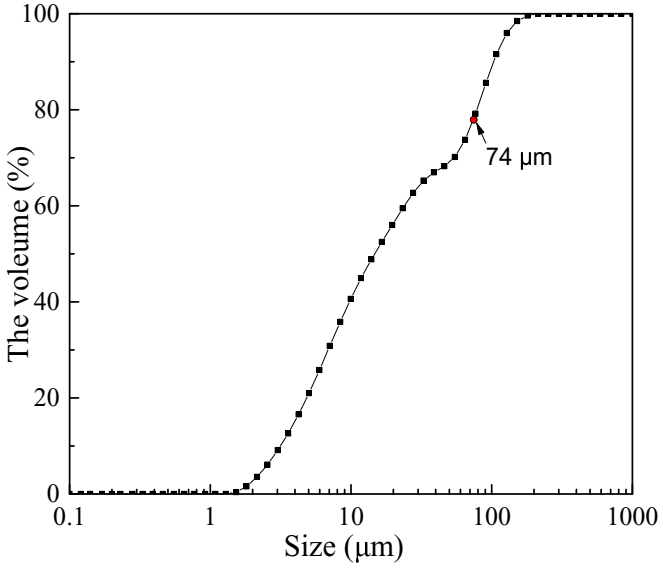

Fig. 7. Size distribution of CS.

Table 7
XRD-Rietveld quantitative analysis of the mineral phase in the rings (mass ratio, %).

Phase	Chemical Formula	Quantitative Analysis
Metallic iron	Fe	9.2
Wustite	FeO	47.5
Calcium carbonate	$CaCO_3$	31.7
Magnesium ferrite	$MgFe_2O_4$	4.8
Zinc ferrite	$ZnFe_2O_4$	6.7

characterization, it can be concluded that CS has a high content of Fe and CaO, which can be considered as a good raw material for iron ore sintering. The utilization of CS in iron ore sintering can replace parts of the iron ore and the flux to achieve the goals of saving energy and lower the cost. Notably, CS also has a high content of $ZnFeO_4$.

3.3.1. Microstructure of CS

Fig. 9 illustrated the typical microstructure of CS obtained by SEM-EDS. Most of the particles contained globular Fe-metals. Magnetite particles often coagulate to form a sphere. From the analysis of XRD and SEM, it can be seen that metallic iron and iron

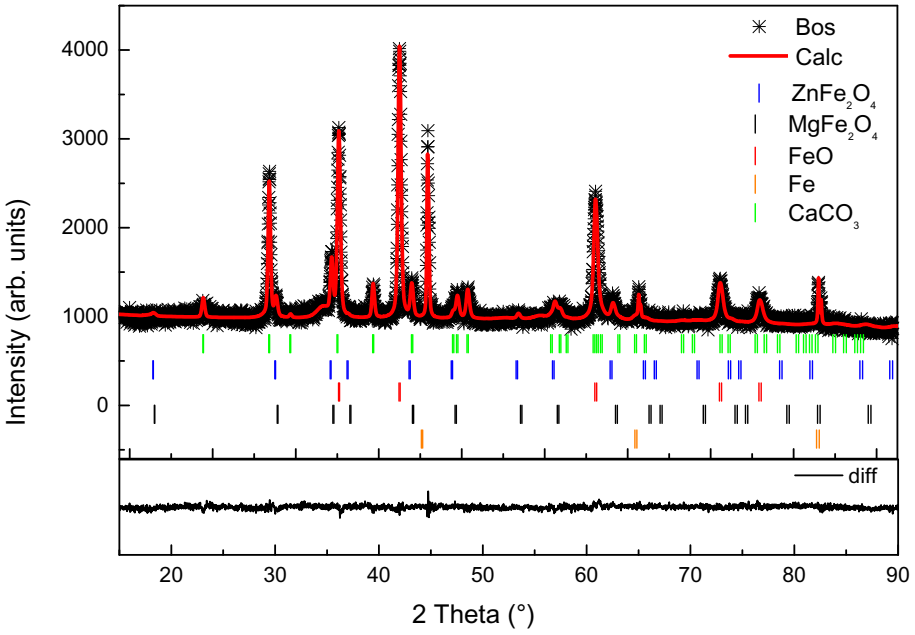

Fig. 8. Rietveld refinement of the observed XRD pattern for the CS.

the equation analog effect was good. The average composition of mineral phases was obtained through multiple tests as shown in Table 7. The results indicate that the main minerals are metallic iron (Fe), wustite (FeO), calcium carbonate ($CaCO_3$), magnesium ferrite ($MgFe_2O_4$), and zinc ferrite ($ZnFe_2O_4$). The XRD-Rietveld analysis suggests that CS contains 9.2% metallic iron, and Fe element mainly exists in the form of wustite. The $CaCO_3$ is second in mass (31.7%), which indicates the high basicity of CS. From the above oxides exist independently in CS. The iron oxides wrapped the metallic Fe with less eutectic mineral, and other impurities such as CaO, MgO and $ZnFe_2O_4$ mixed in the way of physical accumulation. EDS mappings in Fig. 10 further confirmed the elements distribution of Si, Fe, Mg, Ca, C, Cr, and Zn within the CS. The results suggested that much of Ca, Si, Mg, Zn, and Cr were in oxide forms. Part of Ca and Si appeared in the form of composite oxides. Fe found in CS was in form of iron oxide and metallic iron, and there was a

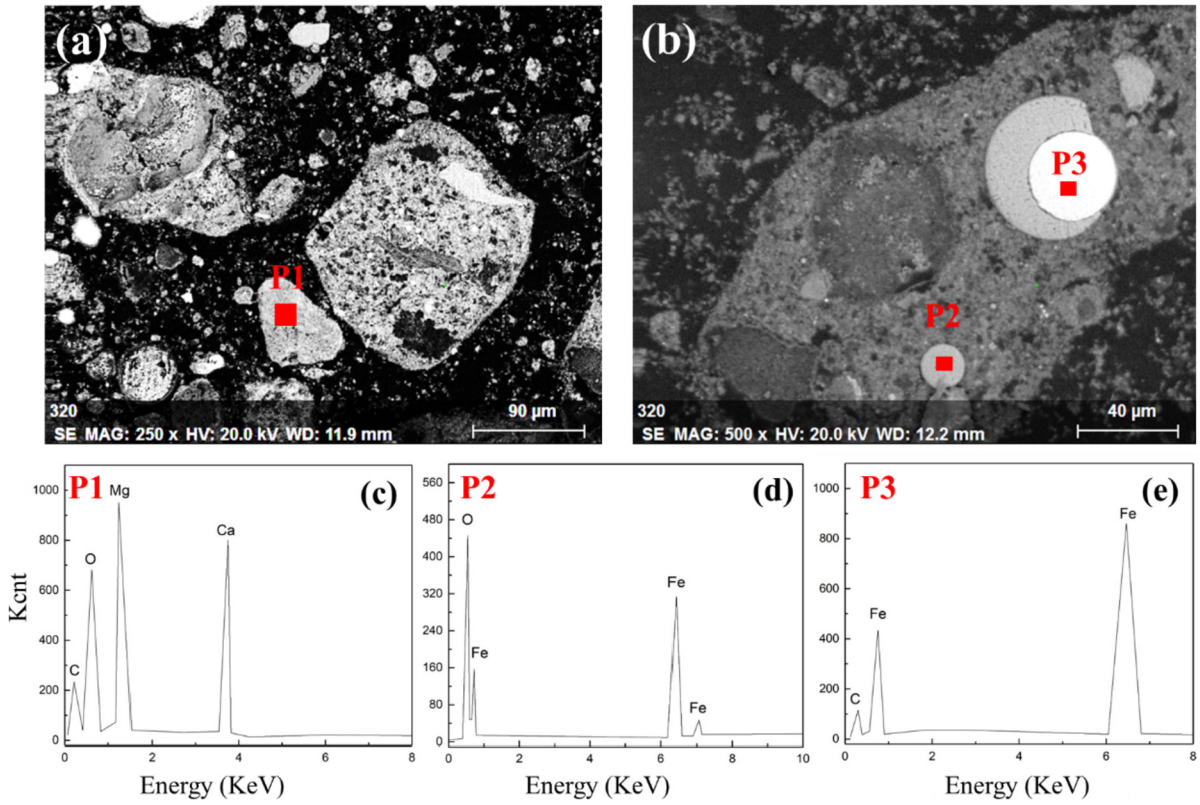

Fig. 9. SEM and EDS maps of CS. (a, b) are the SEM patterns of CS. (c–e) are the EDS patterns of P1, P2, and P3, respectively.

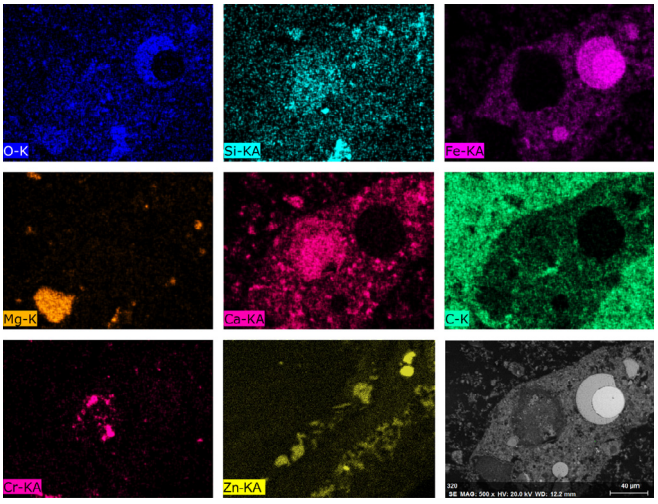

Fig. 10. EDS mappings of CS.

distinct interface between the two phases.

3.4. Moisture capacity and granulation performances

3.4.1. Moisture capacity of iron ore

Moisture capacity, proposed by Lv et al. (Lv et al., 2010b; Mao et al., 2013) for the prediction of appropriate water content in the pelleting process, is used to characterize the interaction between iron ore and water. It is defined as the maximum amount of water that can be contained per unit mass of dried ore under a certain pressure, temperature and accumulation state. Fig. 11 displays the moisture capacity variation of iron ores with different CSDW concentration. The results indicated that the moisture capacity showed a decrease tendency with different degrees in each iron ore. Ores have different sensitivity level to CSDW concentration conditions, and the decline ranges from 0.26% to 19.40%. Equation (2) expressed the water absorption mathematical model proposed by Lv et al. (2010a). S is saturation, %; γ is the surface tension, N/m; r is diameter of tube or pore, m; θ is the contact angle between the water and the iron ore, rad; t is the time, s; μ is the liquid viscosity, Pa S; l_{max} is the maximum length of liquid in the tube, m. For the moisture capacity of a specific ore with different CSDW concentration, θ, t, and l_{max} were roughly constant. Saturation was generally determined by the surface tension and the liquid viscosity. Fig. 12 gives the surface tension of CSDW with different concentrations. The results indicated that the surface tension decreased from 72.81 mN/m to 65.64 mN/m with increasing CSDW concentration. On the other hand, the increase of CSDW concentration could increase the suspended particles in the solution and improve the viscosity of the solution (Ren et al., 2012). As a result, the variation of surface tension and viscosity finally decreased the moisture capacity of the ore. Generally, the moisture capacity can accurately represent the reasonable water content during granulation. With the decrease of moisture capacity, the optimal water content required for the excellent air permeability of the material bed should also be reduced, which indicates a water-saving potential for iron ore sintering.

$$S = \sqrt{(\gamma \cdot r \cdot \cos\theta \cdot t)/(2\mu)/l_{max}} \quad (2)$$

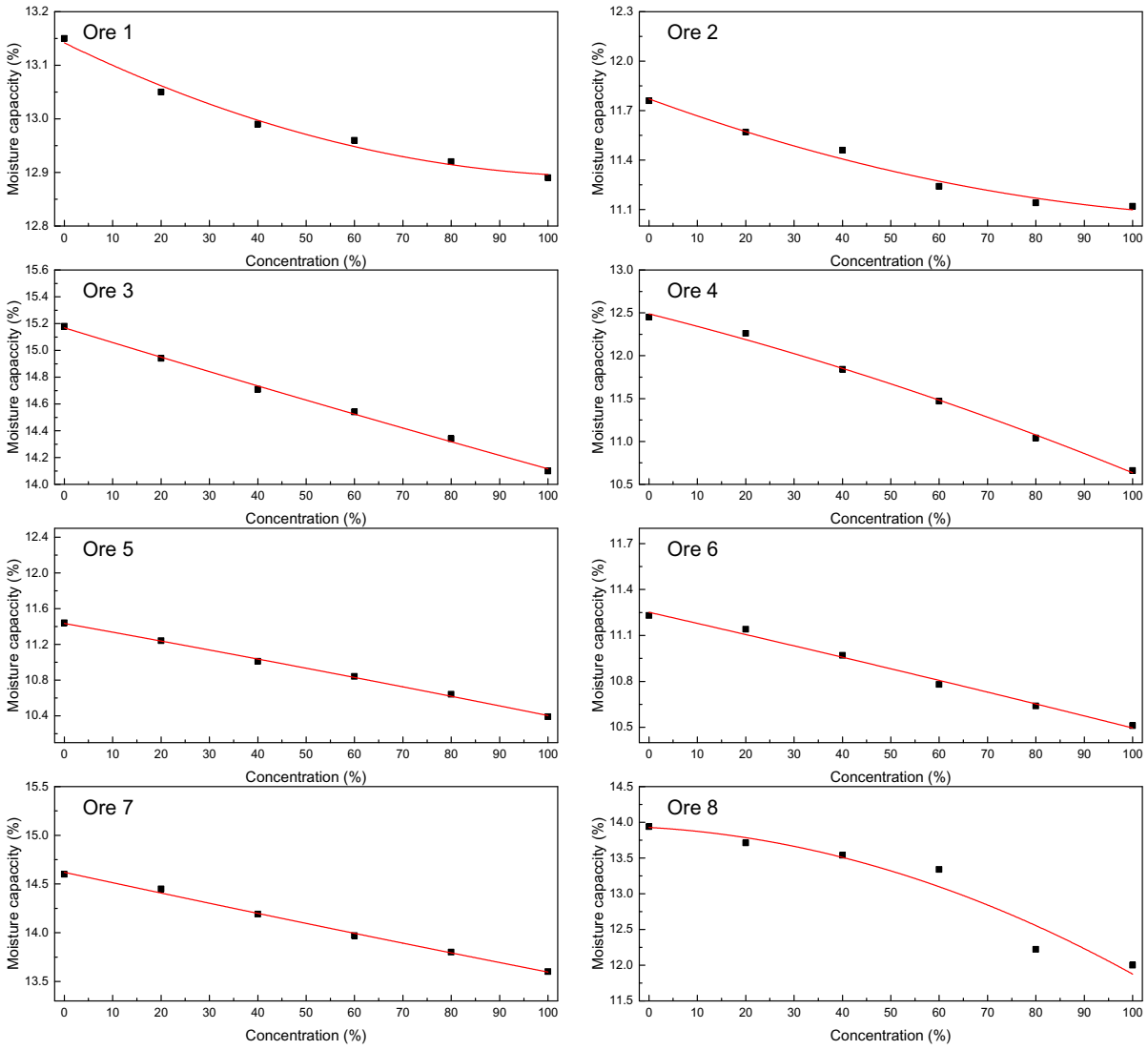

Fig. 11. Moisture capacity of iron ore with different CSDW concentration.

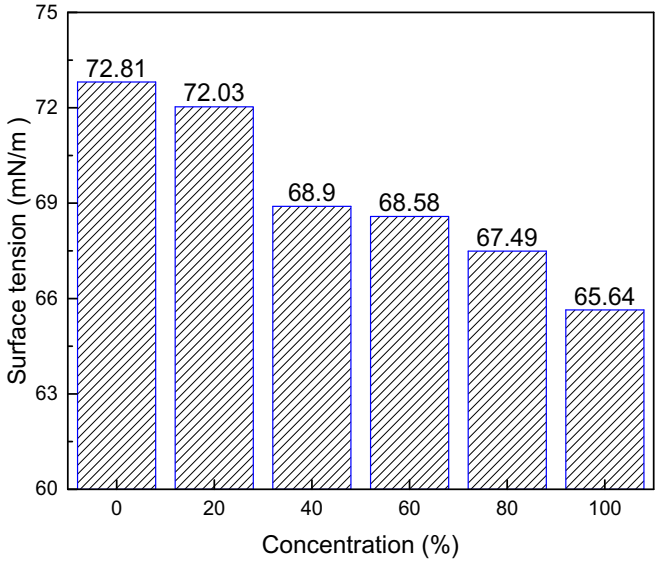

Fig. 12. Surface tension of CSDW with different concentrations.

3.4.2. Granulation performance of iron ore

It is widely believed that higher green feed and sintering permeability can be achieved with better granulation (Litster and Waters, 1988; Oyama et al., 2005; Umadevi et al., 2009). And it will eventually impact the coke combustion efficiency, pollutant emissions, and sinter performance. Fig. 13 (a) gives the particles size distribution of the mixture after granulation. The results indicated that the mass of the +6.13 mm particles increased with CSDW concentration. Generally, Uniformity Index (UI) (Wu et al., 2018) and Japanese Permeability Units (JPU) (Nyembwe et al., 2016) are used to evaluate the granulation performance of the mixture. UI reflected the concentrated distribution degree of the mixture, and the higher the value, the better permeability of the material layer will be (Wu et al., 2018). As expressed in equation-3, UI indicates the content of quasi-particles in the mixture with the particle size of 3–8 mm, $m_{3\text{-}8}$ represents the mass of the particles with the size of 3–8 mm; m_0 represents the total weight of mixture. Fig. 13 (b) illustrated UI values with different concentration of CSDW. With increasing of CSDW concentration, UI first raised and then dropped, and reached the maximum when the CSDW concentration was 40%. JPU reflects the bed permeability of the sinter feeds and can be calculated by using equation-4, where Q is the air

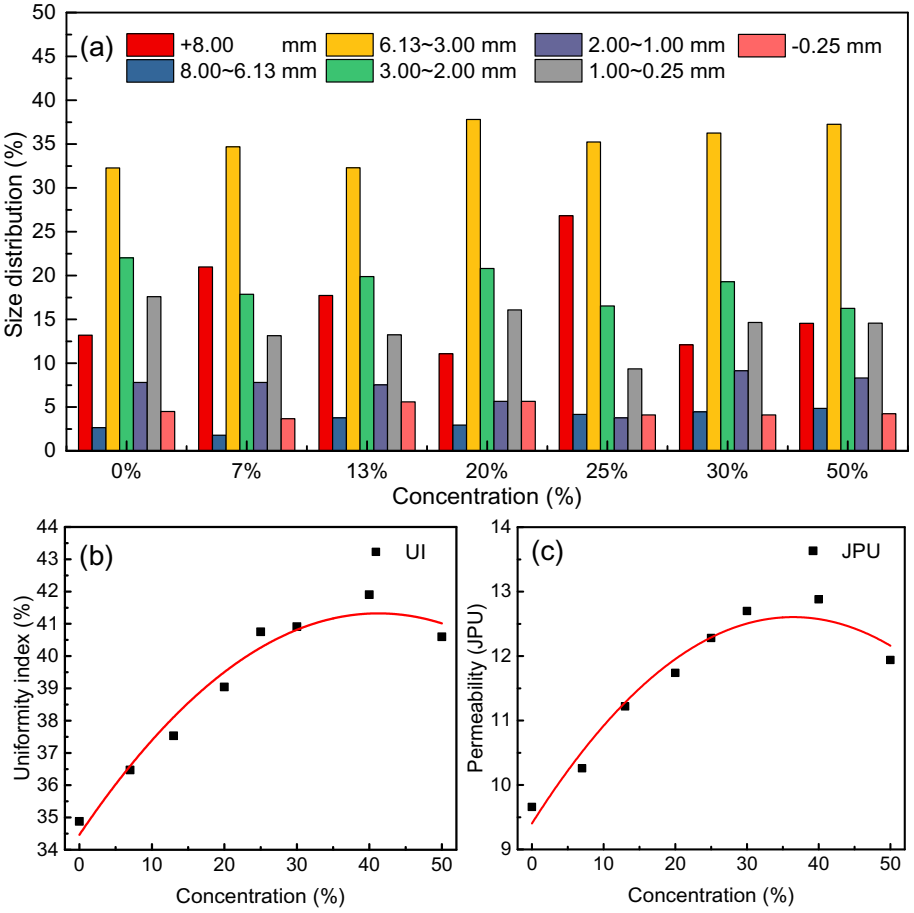

Fig. 13. Effect of CSDW concentration on sintering granulation. (a) The size distribution of particles; (b) UI of the mixture; (c) JPU of the mixture.

flow rate ($m^3 \cdot min^{-1}$); A is the cross-sectional area of the material bed (m^2); H is bed height (mm); △P is the pressure drop (mm H_2O) across the bed (CE, 2003; Ellis et al., 2007; Voice et al., 1953). As can be seen in Fig. 13 (c), the changes of JPU are closely related to UI. With the concentration of CSDW increasing from 0–50%, the permeability firstly raised from 9.66 to 12.88 JPU, and then reduced to 11.94 JPU. This is mainly because CSDW has lower surface tension than fresh water, which leads to the decrease of the moisture capacity. Therefore, under the same moisture content, more water forms capillary water on the surface of the mixture. For the pelleting process of iron ore, the capillary force plays a dominant and decisive role in the various forces (Forsmo et al., 2008, 2006). As a result, UI grew as the CSDW concentration increased. In addition, due to the fine particles size of the CS, it is easy for CS to adhere to the surface of the mixture and promote the pelleting process. However, further increase of CSDW concentration over 40% could reduce the UI and JPU of the mixture. This is because the particles are completely surrounded by water and the capillary force between the particles is sharply weakened. Under this condition, the mixture appeared to be a highly deformable mud, which is difficult for the particles to form a ball.

$$UI = \frac{m_{3-8}}{m_0} \times 100\% \tag{3}$$

$$JPU = \frac{Q}{A}\left(\frac{H}{\Delta P}\right)^{0.6} \tag{4}$$

3.5. Influence of CSDW concentration on sintering indexes

3.5.1. Microstructures of sinter

Fig. 14 shows the microstructures of sinter studied by SEM-EDS. In the sinter (Fig. 14 (a)), hematite interweaved with magnetite and calcium ferrite were the major phrase of the sinter. With the increase of CSDW concentration from 7% to 30%, more calcium ferrite (Fig. 14 (b, P2)) and less skeletal hematite was found in sinter. This is mainly because the increase of CSDW concentration enhance the gas permeability of bed material and improve the oxygen potential during sintering, which is conducive to the formation of calcium ferrite (Jeon et al., 2010; Webster et al., 2013). Owing to the excellent reducibility and consolidation strength of calcium ferrite, this mineral could improve the bonding strength and enhance the reduction index of the sinter (Wang et al., 2019). When the CSDW concentration exceeded 40%, much of secondary hematite was found in sinter, as shown in Fig. 14 (g, h, P6, P7). The excellent permeability of bed material with CSDW concentration also leads to a great quantity heat loss. The rapid cooling of the sinter caused the incomplete transition of hematite phase. A large number of studies (Donskoi et al., 2018; Mizutani et al., 2018; Shuang-ping et al., 2016) showed that volume expansion occurred during the reduction of this hematite, which was bad for the cold strength and low-temperature reduction disintegration of sinter.

3.5.2. Sintering indexes

Maximum exhaust gas temperature, average vertical sintering rate, yield, and tumbler strength are important sintering indexes to

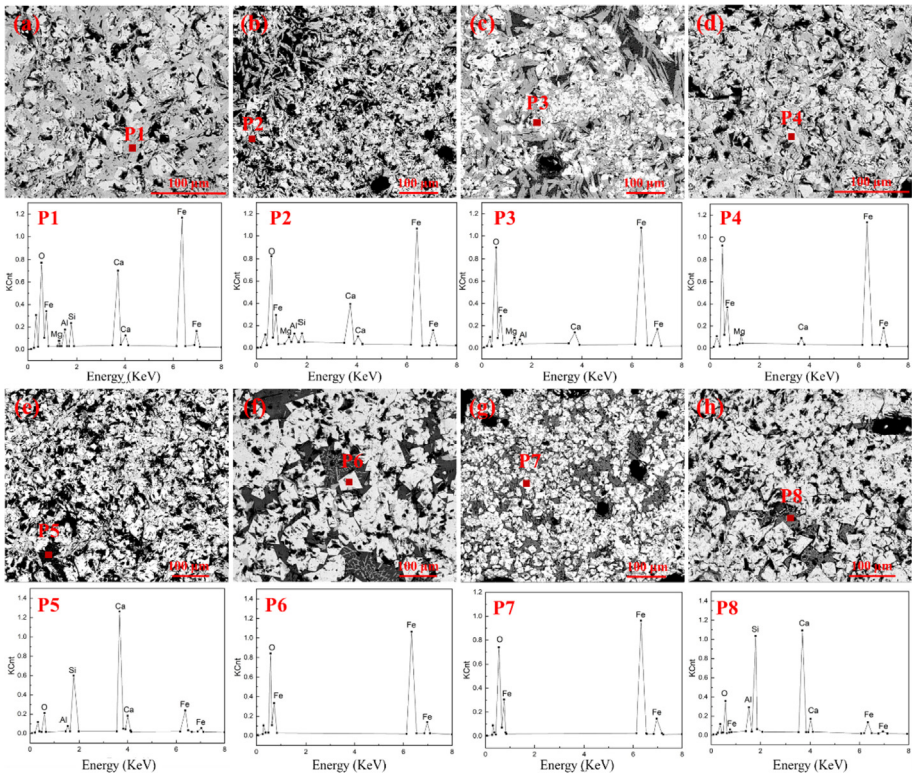

Fig. 14. Microstructure of sinters with different CSDW concentration. (a) 0%; (b) 7%; (c) 15%; (d) 20%; (e) 25%; (f) 30%; (g) 40%; (h) 50%; (P1–P8) EDS maps of P1–P8; P1 and P2, calcium ferrite; P3 and P4, hematite. P5 and P8, slag; P6 and P7 skeletal hematite.

evaluate the sinter quality, as illustrated in Fig. 15. Maximum exhaust gas temperature was usually used to characterize the combustion of the coke breeze and judge the end-point of sintering. As shown in Fig. 15 (a), with increasing of CSDW concentration, the maximum exhaust gas temperature first raised from 413 to 453 °C and then dropped to 449 °C. The results indicated that the increase of CSDW concentration could improve fuel combustion efficiency, which also means higher heat loss during sintering. As expressed in Fig. 15 (b), the average vertical sintering rate changed in the same trend. This was mainly because the increase of CSDW concentration could enhance the gas permeability and improve the oxygen potential during sintering, which improved the efficiency of fuel combustion and accelerated the vertical sintering rate. The yield and the tumbler index (TI) reveal the ambient temperature strength of the sinter, which gives a measurable indicator of its collision resistance during the transfer process. As shown in Fig. 15(c and d), the yield and the tumbler index increased firstly and then decreased with the CSDW concentration increased, and reached the maximum when the concentration was 30%. When CSDW concentration was 30%, the yield and the tumbler strength achieved the maximum value 83.97% and 69.01%, respectively. The evolution of microstructure in Fig. 15 was consistent well with the experiments. With the increase of CSDW concentration from 7% to 30%, more calcium ferrite in sinter improve the strength of the sinter. While the secondary hematite was bad to the strength and yield of the sinter when CSDW concentration exceeded 40%.

3.6. Migration behaviors of harmful elements

3.6.1. Removal rate of harmful elements

CSDW has a high content of hazardous substance, such as ZnO, K_2O, Na_2O, and Cl, which may be problematical for the production process and the ecological environment (Cheng and Chiu, 2003; Oguz, 2004). In order to characterize the migration behavior of harmful elements, theoretical and measured values of harmful elements in sinter were illustrated in Fig. 16. The theoretical values were calculated according to the scheme of ore blending in Table 4 based on the conservation of matter. The calculation in Fig. 16 showed that with the increase of CSDW concentration, the content of ZnO, K_2O, Na_2O and Cl in sinter had the varying degrees of increase. ZnO increased from 0.040% to 0.236%; K_2O increased from 0.116% to 0.121%. Na_2O increased from 0.132% to 0.138%; Cl increased from 0.0015% to 0.0065%. Interestingly, ZnO increased sharply when CSDW was used during sintering, which indicated that ZnO in sinter mainly came from CS. Notably, Cl in sinter came from DW and the content of Cl remained nearly at a constant level. This is mainly because the amount of DW remains constant with the increase of CSDW. By contrast, the calculated values of K_2O and Na_2O did not change significantly with the increase of CSDW. The measurement results showed that after sintering, ZnO, K_2O, Na_2O, and Cl in sinter were greatly reduced. ZnO fluctuated within the range of 0.03–0.06%; K_2O fluctuated within the range of 0.01–0.10%; Na_2O fluctuated within the range of 0.09–0.13%; Cl in sinter was about 0.01%. By comparing the theoretical values with the measured values, it can be found that harmful elements content decreased to a certain extent by using CSDW. The removal rates (γ) are calculated according to equation-5, where M_t represents the theoretical content; M_m represents the measured content. Fig. 16 (e) expressed the removal rates of different elements. With the increase of CSDW concentration, the removal rate of ZnO, K_2O, and Na_2O increased from 23% to 74%, 13%–42%, 1%–34%, respectively. The removal rates of Cl remained 83%. The results indicated that the removal rates were different among the harmful elements in order: Cl > Zn > K > Na.

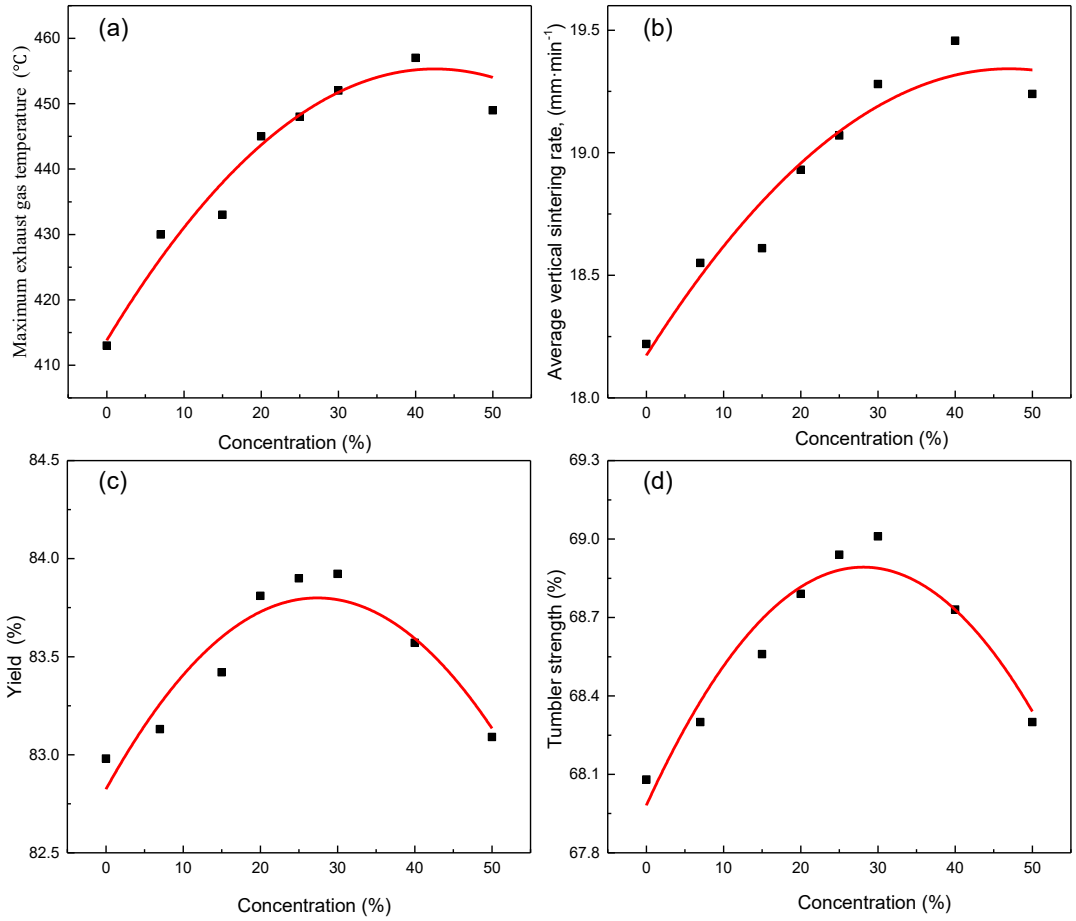

Fig. 15. Effect of CSDW concentration on sintering indexes. (a) Exhaust gas temperature; (b) Vertical sintering rete; (c) Yield; (d) Tumbler strength.

$$\gamma = \frac{M_t - M_m}{M_t} \times 100\% \quad (5)$$

3.6.2. Removal mechanisms of harmful elements

The sintering process involves complex chemical reactions. Therefore, it is very important to study the reactions thermodynamics of the alkali oxides during sintering. Under a certain temperature, low P_{O_2} means low oxygen potential of the oxide, low Gibbs free energy $\Delta_r G_m^{\varnothing}$, and high oxide stability. In the coupled redox reaction, the oxygen released by one oxide is always absorbed to form another oxide. Therefore, the standard Gibbs free energy can be used as the standard to judge the relative stability of the oxide. The standard Gibbs free energy can also be expressed as equation (6).

$$\Delta_r G_m^{\varnothing} = \Delta_r H_m^{\varnothing} - T\Delta_r S_m^{\varnothing} \quad (6)$$

$\Delta_r H_m^{\varnothing}$ and $\Delta_r S_m^{\varnothing}$ represent the average value of change in enthalpy and change in entropy, respectively. $\Delta_r H_m^{\varnothing}$ and $\Delta_r S_m^{\varnothing}$ are weakly dependent on the temperature or the changes are roughly offset by each other, and they could be recognized as constant. Therefore, the standard Gibbs free energy curves of oxides in CSDW at different temperatures can be obtained through the above calculation, and the results are shown in Fig. 17. The reduction temperatures of alkali metal oxides by C and CO under standard conditions were illustrated in Table 8. The results indicated that K_2O, K_2CO_3, Na_2O and Na_2CO_3 can be easily reduced by CO and C under sintering temperature. The generated alkali vapor can be carried into the flue by the airflow to realize removal goals. Compared with the reduction of Na_2O, the reduction of K_2O is easier, which indicates that K_2O has a higher removal rate than Na_2O during sintering. However, many literature reported that K and Na in iron ore are mainly existed in form of $KAlSi_2O_6$ and $NaAlSi_2O_6$ (Chen et al., 2018; Fernández-González et al., 2017; Tsubouchi et al., 2006). Thermodynamic calculations show that $KAlSi_2O_6$ and $NaAlSi_2O_6$ cannot be reduced under sinter temperature, which suggests that it is difficult to remove K and Na from the mixture by reduction. This also explains the low removal rate of K and Na without CSDW in Fig. 16 (e). As shown in Table 8, the reduction of ZnO and $ZnFe_2O_4$ by C can be easily occurred at the temperature of 952 °C and 1016 °C. Consider that the vapor pressure of the gaseous Zn in Fig. 17 is 1 bar. Under real conditions, Zn vapor pressure in the gas phase is much lower. This means the ZnO and $ZnFe_2O_4$ can be reduced by lower temperature. The research in 3.1 indicated that CS has a high level of $ZnFe_2O_4$ and C. During the sintering process, $ZnFe_2O_4$ in the CS are easily reduced by the C self-contained in the sludge, and the generated Zn is taken away by the airflow.

The mixture also has a high proportion of Cl from DW. Fig. 16 (e) indicated that the removal rate of Cl in the mixture was over 80%. Fig. 18 summarized the possible chemical reactions of Cl. Under high-temperature conditions, Cl in water can form HCl. As shown in Fig. 18, the HCl produced by the volatilization of Cl can react with Na_2CO_3, K_2CO_3, $NaAlSi_2O_6$, and $KAlSi_2O_6$ to generate NaCl and KCl. Compared with $NaAlSi_2O_6$ and $KAlSi_2O_6$, the results show that the

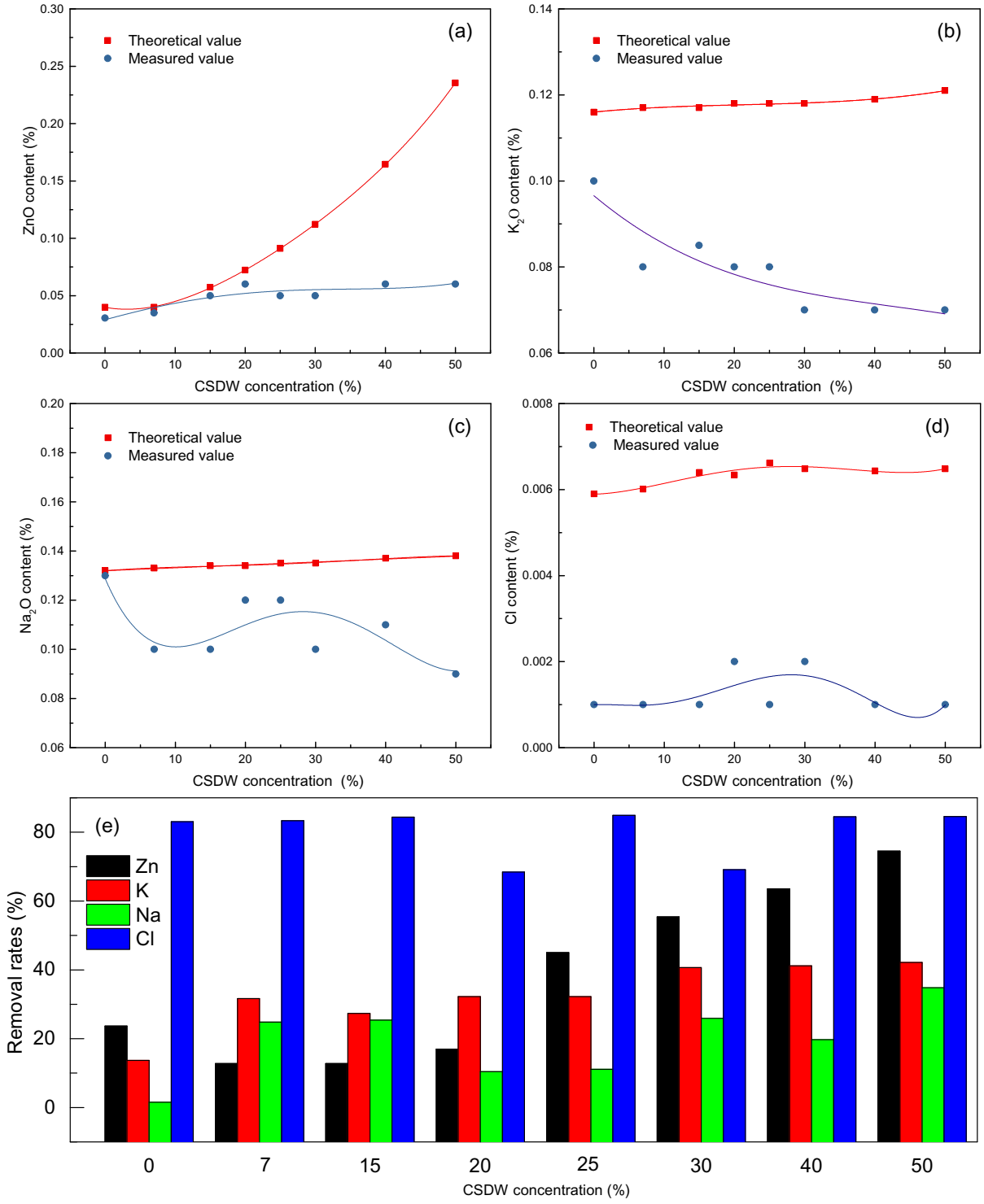

Fig. 16. Theoretical and measured values of harmful elements in sinter. (a) ZnO; (b) K_2O; (c) Na_2O; (d) Cl; (e) Removal rates.

reactions of HCl with Na_2O_3 and K_2CO_3 are easier. Under the oxidizing atmosphere, HCl can also react with oxygen to form Cl_2. Thermodynamic calculations show that Cl_2 can easily react with Na_2CO_3 and K_2CO_3 to form NaCl and KCl under reducing atmosphere. Furthermore, Cl_2 can react with $NaAlSi_2O_6$ and $KAlSi_2O_6$ to form NaCl and KCl. The produced NaCl and KCl were partially carried away by the sintering gas stream during sintering, and the rest was retained in sinter. It can be seen that the Cl introduced by the DW can be removed in form of HCl or Cl_2. As shown in Fig. 19, the generated HCl and Cl_2 could react with Na_2O_3, K_2CO_3, $NaAlSi_2O_6$, and $KAlSi_2O_6$ to form NaCl and KCl during sintering, thereby promoting the removal of alkali metals. That explained well why the removal rates of K and Na were significantly increased when CSDW was used. In brief, the co-utilization of converter sludge-containing dedust wastewater in iron ore sintering could promote the removal of K and Na, and the produced sinter meets the requirements of blast furnace smelting.

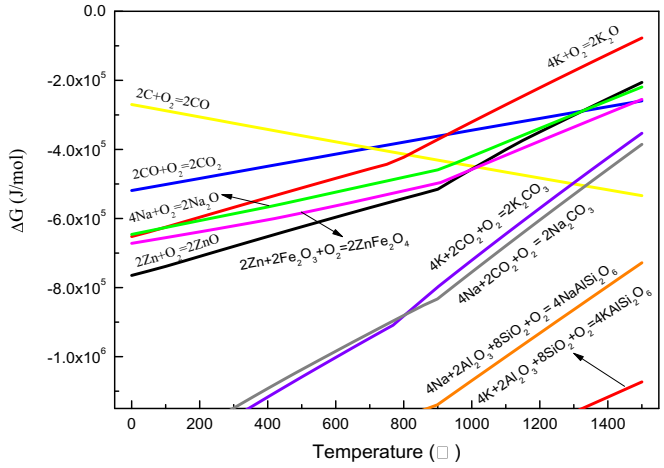

Fig. 17. Standard Gibbs free energy curves of oxides in CSDW with different temperatures.

Table 8
Reduction temperature of alkali metal oxides under standard conditions.

Reduction equation	Temperature, °C
$K_2O + C = 2\,K + CO$	$T \geq 813$
$K_2O + CO = 2\,K + CO_2$	$T \geq 928$
$K_2CO_3 + C = 2\,K + CO + CO_2$	$T \geq 1296$
$K_2CO_3 + CO = 2\,K + 2CO_2$	$T > 1500$
$2KAlSi_2O_6 + CO = 2\,K + Al_2O_3 + 4SiO_2 + CO_2$	$T > 1500$
$2KAlSi_2O_6 + C = 2\,K + Al_2O_3 + 4SiO_2 + CO$	$T > 1500$
$Na_2O + C = 2Na + CO$	$T \geq 1011$
$Na_2O + CO = 2Na + CO_2$	$T \geq 1325$
$Na_2CO_3 + CO = 2Na + 2CO_2$	$T \geq 1335$
$Na_2CO_3 + CO = 2\,Na + 2CO_2$	$T > 1500$
$2NaAlSi_2O_6 + CO = 2Na + Al_2O_3 + 4SiO_2 + CO_2$	$T > 1500$
$2NaAlSi_2O_6 + C = 2Na + Al_2O_3 + 4SiO_2 + CO$	$T > 1500$
$ZnO + C = Zn + CO$	$T \geq 952$
$ZnO + CO = Zn + CO_2$	$T \geq 1325$
$ZnFe_2O_4 + C = Zn + Fe_2O_3 + CO$	$T \geq 1016$
$ZnFe_2O_4 + CO = Zn + Fe_2O_3 + CO_2$	$T \geq 1481$

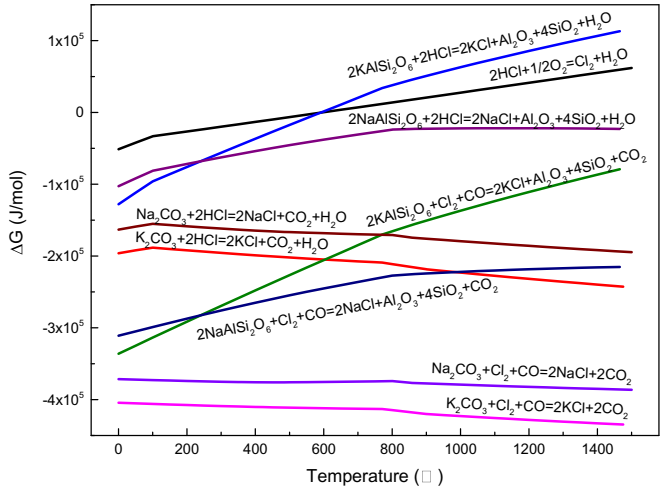

Fig. 18. Standard Gibbs free energy curves of compounds (Cl, K, and Na) with different temperatures.

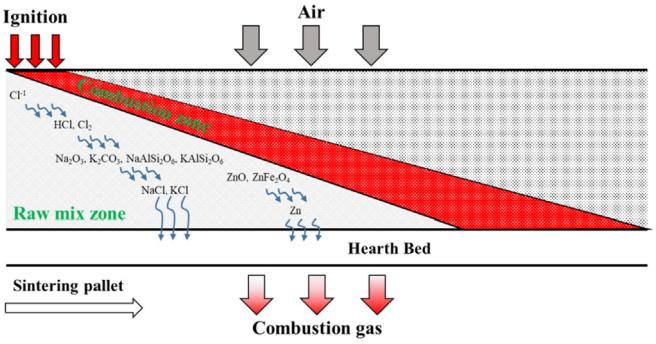

Fig. 19. Schematic diagram of harmful elements migration during sintering.

4. Conclusion

This paper aims to provide a new method for the co-utilization of CSDW in iron ore sintering to overcome the problem of high composition fluctuate and high harmful elements in sinter. The main findings were summarized as follows.

(1) The proportion of the CS particles (<74 μm) accounted for more than 80%. The XRD-Rietveld analysis suggests that the main minerals are metallic iron (9.2%), wustite (47.5%), calcium carbonate (31.7%), magnesium ferrite (4.8%), and zinc ferrite (6.7%). CaO, MgO, Fe, and $ZnFe_2O_4$ are mixed in the way of physical accumulation with less eutectic mineral in the CS.

(2) The increase of CSDW concentration could reduce the surface tension from 72.81 mN/m to 65.64 mN/m and improve the liquid viscosity, which finally decreased the moisture capacity of the ore. The granulation experiments indicated that UI raised firstly and then dropped, and the highest group was the concentration of 40%. Closely related to UI, the permeability firstly raised from 9.66 to 12.88 JPU and then reduced to 11.94 JPU.

(3) With the increase of CSDW concentration from 7% to 30%, more calcium ferrite was found in sinter. When the CSDW concentration exceeded 40%, much of the secondary hematite formed. The rapid cooling of the sinter caused the incomplete transition of hematite phase. When CSDW concentration was 30%, the yield and the tumbler strength achieved the maximum value of 83.97% and 69.01%, respectively.

(4) ZnO and $ZnFe_2O_4$ in CS can be easily reduced by the C self-contained in the sludge, and the generated Zn is taken away by the airflow. The generated HCl and Cl_2 can react with Na_2O_3, K_2CO_3, $NaAlSi_2O_6$, and $KAlSi_2O_6$ to form NaCl and KCl during sintering, thereby promoting the removal of alkali metals. The removal rate of ZnO, K_2O, and Na_2O increased from 23% to 74%, 13%–42%, 1%–34%, respectively. The removal rates of Cl remained 83%. Under the CSDW concentration of 30%~40%, the quality of the sinter could be improved. The harmful elements could be removed and collected during sintering, which is conducive to realize the goals of saving fresh water, enhancing quality and reducing pollution.

Acknowledgement

The authors acknowledge the support of Major Science and Technology Program for Water Pollution Control and Treatment under Grant (2017ZX07402001), the National Natural Science

Foundation of China (51874025), and National Key R&D Program of China (2017YFB0304300 & 2017YFB0304302). Yaozu Wang gratefully acknowledges financial support from China Scholarship Council for one year study at the Montanuniversitaet Leoben, Austria.

References

Agrawal, R.K., Pandey, P.K., 2005. Productive recycling of basic oxygen furnace sludge in integrated steel plant. J. Sci. Ind. Res. (India) 64, 702–706.
Aihua, W., Pinggang, W., Zhoulian, H., Pan, L., Lixin, J., n.d. Produce of Iron Powder Using Sludge Coarse Particles 1–5.
Bartels, W.J., Hornstra, J., Lobeek, D.J.W., 1986. X-ray diffraction of multilayers and superlattices. Acta Crystallogr. A 42, 539–545.
Cantarino, M.V., Filho, C.D.C., Mansur, M.B., 2012. Hydrometallurgy Selective removal of zinc from basic oxygen furnace sludges. Hydrometallurgy 111–112, 124–128. https://doi.org/10.1016/j.hydromet.2011.11.004.
CE, L., 2003. Quantifying the resistance to airflow during iron ore sintering. ISIJ Int. 43, 630–636.
Chen, D., Gou, H., Lv, Y., Li, P., Yan, B., Xu, J., 2018. Preparation and recovery of iron carbide from pyrite cinder using carburization-magnetic separation technology. J. Min. Metall. Sect. B Metall. 54.
Cheng, T.-W., Chiu, J.P., 2003. Fire-resistant geopolymer produced by granulated blast furnace slag. Miner. Eng. 16, 205–210.
da Silva, R.R., de Carvalho Mathias, F.R., Bajay, S.V., 2018. Potential energy efficiency improvements for the Brazilian iron and steel industry: fuel and electricity conservation supply curves for integrated steel mills. Energy 153, 816–824.
Das, B., Prakash, S., Reddy, P.S.R., Misra, V.N., 2007. An overview of utilization of slag and sludge from steel industries. Resour. Conserv. Recycl. 50, 40–57.
Denk, M., Gläßer, C., Kurz, T.H., Buckley, S.J., Drissen, P., 2015. Mapping of iron and steelwork by-products using close range hyperspectral imaging: a case study in Thuringia, Germany. Eur. J. Remote Sens. 48, 489–509. https://doi.org/10.5721/EuJRS20154828.
Donskoi, E., Manuel, J.R., Lu, L., Holmes, R.J., Poliakov, A., Raynlyn, T.D., 2018. Importance of textural information in mathematical modelling of iron ore fines sintering performance. Miner. Process. Extr. Metall. 127, 103–114.
Ellis, B.G., Loo, C.E., Witchard, D., 2007. Effect of ore properties on sinter bed permeability and strength. Ironmak. Steelmak. 34, 99–108.
Fernández-González, D., Ruiz-Bustinza, I., Mochón, J., González-Gasca, C., Verdeja, L.F., 2017. Iron ore sintering: Process. Miner. Process. Extr. Metall. Rev. 38, 215–227.
Forsmo, S.P.E., Apelqvist, A.J., Björkman, B.M.T., Samskog, P.-O., 2006. Binding mechanisms in wet iron ore green pellets with a bentonite binder. Powder Technol. 169, 147–158.
Forsmo, S.P.E., Samskog, P.-O., Björkman, B.M.T., 2008. A study on plasticity and compression strength in wet iron ore green pellets related to real process variations in raw material fineness. Powder Technol. 181, 321–330.
Hao, T., 2005. Utilization of inplant reclaimed dust slurry in tanggang 210m2 sintering plant. Sinter. Pelletizing 4, 34.
Jeon, J.-W., Jung, S.-M., Sasaki, Y., 2010. Formation of calcium ferrites under controlled oxygen potentials at 1273 K. ISIJ Int. 50, 1064–1070.
Jin, Z., Liu, J., 2006. Service test of guniting high concentration OG sludge in Masteel. Anhui Metall 3, 0.
Lanzerstorfer, C., Bamberger-Strassmayr, B., Pilz, K., 2015. Recycling of blast furnace dust in the iron ore sintering process: investigation of coke breeze substitution and the influence on off-gas emissions. ISIJ Int. 55, 758–764.
Lei, H., Li, K., 2015. Application of sludge pellet in converter steelmaking. China Metall 25, 8–11.
Leiviskä, T., Khalid, M.K., Sarpola, A., Tanskanen, J., 2017. Removal of vanadium from industrial wastewater using iron sorbents in batch and continuous flow pilot systems. J. Environ. Manag. 190, 231–242.
Litster, J.D., Waters, A.G., 1988. Influence of the material properties of iron ore sinter feed on granulation effectiveness. Powder Technol. 55, 141–151.
Lv, X., Bai, C., Qiu, G., Hu, M., 2010a. Kinetics of water absorption by the bed of iron ore particles during granulation. Powder Technol. 204, 138–144.
Lv, X., Bai, C., Qiu, G., Zhang, S., Hu, M., 2010b. Moisture capacity: definition, measurement, and application in determining the optimal water content in granulating. ISIJ Int. 50, 695–701.
Mao, H., Zhang, R., Lv, X., Bai, C., Huang, X., 2013. Effect of surface properties of iron ores on their granulation behavior. ISIJ Int. 53, 1491–1496.
Melali, A.R., Shariatmadari, H., 2008. Application of steel making slag and converter sludge in farm manure enrichment for corn nutrition in greenhouse conditions. JWSS-Isfahan Univ. Technol. 11, 505–513.
Mizutani, M., Nishimura, T., Orimoto, T., Higushi, K., Nomura, S., Saito, K., Kasai, E., 2018. Quantitative evaluation of reaction mode and reduction disintegration behavior of iron ore agglomerates during low temperature reduction. ISIJ Int. 58, 1761–1767.
Nolasco-Sobrinho, P.J., Espinosa, D.C.R., Tenório, J.A.S., 2003. Characterisation of dusts and sludges generated during stainless steel production in Brazilian industries. Ironmak. Steelmak. 30, 11–17. https://doi.org/10.1179/030192303225009506.
Nyembwe, A.M., Cromarty, R.D., Garbers-Craig, A.M., 2016. Effect of concentrate and micropellet additions on iron ore sinter bed permeability. Miner. Process. Extr. Metall. 125, 178–186.
Oguz, E., 2004. Removal of phosphate from aqueous solution with blast furnace slag. J. Hazard Mater. 114, 131–137.
Oyama, N., Sato, H., Takeda, K., Ariyama, T., Masumoto, S., Jinno, T., FUJII, N., 2005. Development of coating granulation process at commercial sintering plant for improving productivity and reducibility. ISIJ Int. 45, 817–826.
Peng, J., Xie, R., Lai, M., 2018. Energy-related CO2 emissions in the China's iron and steel industry: a global supply chain analysis. Resour. Conserv. Recycl. 129, 392–401.
Ren, S., Zhang, J., Wu, L., Liu, W., Bai, Y., Xing, X., Su, B., Kong, D., 2012. Influence of B2O3 on viscosity of high Ti-bearing blast furnace slag. ISIJ Int. 52, 984–991.
Ren, Z., Liu, H., Chang, X., Tang, Z., 1998. Lime hydration test of converter OG dust and application to sinter production. Iron Steel 33, 4–8.
Shuang-ping, Y., Shuan-quan, G.U.O., Pan-hui, Z., Jiang-feng, Z., Miao, W., 2016. Influence of semi-coke used as sintering fuel on metallurgical properties of sinter. Iron Steel 4.
Su, F., Lampinen, H.O., Robinson, R., 2004a. Recycling of sludge and dust to the BOF converter by cold bonded pelletizing. ISIJ Int. 44, 770–776.
Su, Y., Jin, J., Wang, G., Yi, M., 2004b. Development and application of steelmaking dust directly charging in sinter mixing. Material. China Metall. 6, 18–21.
Tsubouchi, N., Kuzuhara, S., Kasai, E., Hashimoto, H., Ohtsuka, Y., 2006. Properties of dust particles sampled from windboxes of an iron ore sintering plant: surface structures of unburned carbon. ISIJ Int. 46, 1020–1026.
Umadevi, T., Deodar, A.V., Mahapatra, P.C., Prabhu, M., Ranjan, M., 2009. Influence of alumina on iron ore sinter properties and productivity in the conventional and selective granulation sintering process. Steel Res. Int. 80, 686–692.
Voice, E.W., Brooks, S.H., Gledhill, P.K., 1953. The permeabiligy of sinter beds. J. Iron Steel Inst. 174, 136–139.
Wang, Y., Liu, Z., Zhang, J., Du, C., Niu, L., 2019. Central band structures: new insights into the coupling effects between the pores and minerals of sinter. Metall. Mater. Trans. B. https://doi.org/10.1007/s11663-018-01501-z.
Wang, Y.H., Ping, D.U., Ren, L.Q., 2015. Experiment of pelletizer sintering by fine powder and sludge. China Metall 5, 11–14.
Wang, Y.Z., Zhang, J.L., Liu, Z.J., Du, C.B., 2017. Recent advances and research status in energy conservation of iron ore sintering in China. JOM (J. Occup. Med.) 69, 2404–2411.
Webster, N.A.S., Pownceby, M.I., Madsen, I.C., Kimpton, J.A., 2013. Effect of oxygen partial pressure on the formation mechanisms of complex Ca-rich ferrites. ISIJ Int. 53, 774–781.
World steel association, 2018. World Steel in Figures 2018.
Wu, S., Que, Z., Li, K., 2018. Strengthening granulation behavior of specularite concentrates based on matching of characteristics of iron ores in sintering process. J. Iron Steel Res. Int. 25, 1017–1025.
Wu, Z.J., Zhou, Y., Su, S.H., Gao, Z.F., Wu, X.R., Li, L.S., 2012. A novel conversion of converter sludge into amorphous multi-doped FePO4cathode material for lithium ion batteries. Scripta Mater. 67, 221–224. https://doi.org/10.1016/j.scriptamat.2012.04.027.
Zhang, Z.F., Wu, Z.J., Su, S.H., Gao, Z.F., Li, L.S., Wu, X.R., 2013. Sustainable preparation of Li(FeM)PO4/C from converter sludge and its electrochemical performance as a cathode material for lithium ion batteries. J. Alloy. Comp. 574, 136–141. https://doi.org/10.1016/j.jallcom.2013.04.015.
Zhao, J., Zhu, H., 2004. Commercial exprement and production on using steel making directly sludge into sintering directly. J. Anhui Vocat. Coll. Metall. Technol. 14, 23–25.